AIAA SciTech Forum
6-10 January 2020, Orlando, FL
AIAA Scitech 2020 Forum

10.2514/6.2020-1165

Performance evaluation of fan and comb shaped plasma reactors for distribution of generated ozone in a confined space

Bhaswati Choudhury[1], Sherlie Portugal[2], Judith Johnson[3], Subrata Roy[4,5]
Applied Physics Research Group, University of Florida, Gainesville, Florida, 32611, USA

Enhanced distribution of atmospheric surface dielectric barrier discharge (SDBD) generated ozone in air for effective decontamination is examined. This is achieved through experimental measurement and numerical prediction of the flow and ozone distribution produced by surface DBD plasma reactors kept in a closed chamber. This study provides an alternative technique for decontamination of assembly cleanroom facilities and spacecraft components. Conventional methods like dry heat microbial reduction and vapor phase hydrogen peroxide used in spacecraft related decontamination lead to thermal and chemical damage of sophisticated materials. Advantages associated with atmospheric DBD plasma decontamination like low temperatures, no organic-residuals and design flexibility make it a potential alternative to these methods. In this study, spore forming bacterial species, *Bacillus subtilis*, which is commonly used in planetary protection studies was used as the test organism. Significant reduction (~78%) of bacterial concentrations in the inoculated volume of air was observed using the comb shaped DBD plasma reactor. Increased reduction (~98%) was observed when the same reactor was used in conjunction with an external fan for better ozone distribution. Considering this, a recently developed DBD configuration called the fan SDBD reactor can be used instead of the external fan to obtain better ozone distribution leading to lower ozone requirements and energy consumption. For this purpose, ozone distribution in a chamber with the comb and fan SDBD reactor were compared experimentally. The fan SDBD reactor uniformly distributed ozone from the center towards the walls of the chamber with higher ozone concentrations at the center. In contrast, the comb SDBD reactor pushed the ozone towards one of the walls resulting in biased distribution with higher concentrations in one direction. These results suggest that the fan reactor is better suited for decontamination applications like sterilization of space craft components where a more uniform decontamination is preferred requiring less ozone concentrations. Preliminary simulation results of flow and ozone distribution by the comb and fan reactors up till 10 seconds of powering up are validated with experimental data. Such numerical simulations of ozone distribution resulting from different SDBD configurations can be used to develop and optimize reactor configurations for planetary protection decontamination applications.

I. Introduction

Prevention of interplanetary contamination is imperative in space research missions to protect the celestial body of interest from earthly organisms (forward contamination) and the Earth from extra-terrestrial agents (backward contamination). To this effect, the Committee on Space Research (COSPAR) developed international policies for planetary protection which are updated every two years [1]. These policies are based on the celestial body of interest and the type of mission. Planetary protection necessitates decontamination of assembly cleanroom facilities and spacecraft components for reduction (disinfection) or eradication (sterilization) of microbial inhabitants [2]. Among different microorganisms that contaminate spacecraft environments, spore forming bacteria like the *Bacillus* species and facultative anaerobes like *Escherichia coli* are known to be the most resistant microorganisms that endure harsh environments in a dormant state and grow later when conditions become favorable [3, 4]. Such bacterial species are used as test organisms to validate decontamination technologies suitable for space exploration missions [3, 4].

[1] Graduate Research Assistant, Department of Mechanical and Aerospace Engineering, University of Florida, AIAA student member.
[2] Professor, School of Electrical Engineering, Technological University of Panama, AIAA student member.
[3] Retired Professor, Department of Pathology, Immunology and Laboratory Medicine, University of Florida.
[4] Professor, Department of Mechanical and Aerospace Engineering, University of Florida, AIAA Associate Fellow.
[5] President, SurfPlasma, Gainesville Florida, 32601, AIAA Associate Fellow.

Decontamination technologies currently approved for space missions by the National Aeronautics and Space Administration (NASA) and the European Cooperation for Space Standardization (ECSS) include dry heat microbial reduction (DHMR) and vapor phase hydrogen peroxide (VHP) [5-7]. However, these technologies can be detrimental to advanced materials and electronics used in spacecraft development today. The ECSS reported that high processing temperatures used in DHMR lead to the damage of heat sensitive materials while hydrogen peroxide used in VHP can lead to detrimental material alteration [8]. Thus, there is a need for alternative decontamination technologies that can overcome disadvantages of high temperatures and material incompatibility while attaining adequate levels of decontamination.

Non-thermal plasma (NTP), also known as cold atmospheric plasma (CAP), is a promising alternative decontamination technology with advantages like low temperatures, low cost, no organic-residuals and design flexibility [9-11]. NTP is essentially gas which is electrically energized to a state of partial ionization and is characterized by low overall temperatures. Literature shows that NTP decontamination is a potential alternative for conventional methods used in planetary protection [3, 12-13]. Schruerger et al. (2008) [12] reported 6 log reduction in *Bacillus subtilis* spores on six spacecraft materials with no material alteration caused by NTP exposure. Shimizu et al. (2014) [3] reported the inactivation of a variety of bacterial species including endospores and tested the effects of NTP exposure on different spacecraft materials. In addition to sterilization [14-16], NTPs have also been employed in many applications including biomedicine [17-19], medical treatment [20, 21], flow control [22-24] and disinfection of air [25-27], water [14,28,29] and food or food storage [29-31]. Among the different methods available for non-thermal plasma generation, dielectric barrier discharge (DBD) plasma is unique due to its design flexibility, easy set-up, ability to operate in atmospheric conditions, and its influence on the flow patterns of the neighboring fluid [32]. Previous research shows DBD plasma can lead to sterilization of bacterial endospores which is crucial for planetary protection [13,33].

DBD plasma is formed when an AC voltage is applied across two electrodes separated by a dielectric barrier and a gas filled gap. Atmospheric DBD plasma involves ionization of neighboring air resulting in the generation of various reactive species, UV photons and electric fields from local charge distribution [3, 34]. DBD plasma treatment results from direct contact of plasma discharge with the target or indirect contact resulting from the interaction of transported reactive species with the target. In indirect treatments, mobility of the reactive species makes it possible to treat obscured spaces in the target where direct contact is not possible. Among these reactive species, ozone is known to be a major factor responsible for microbial inactivation [35-38]. A lot of studies can be found in current literature on inactivation mechanisms and practical applications of plasma-based ozone decontamination systems [34,39-43]. However, there are few studies which investigate the effect of distribution of the generated ozone on decontamination [36] which can be crucial in developing optimal DBD-plasma decontamination systems. If decontamination can be enhanced with better ozone distribution, the energy lost in DBD flow generation can be utilized to distribute the generated ozone resulting in lower ozone requirements and energy consumption. The idea is to test the effect of ozone distribution on decontamination and employ DBD flow control for distributing the ozone generated. In this study, we will use the comb and fan surface DBD (SDBD) plasma configurations to model SDBD generated ozone distribution. While the comb configuration has been previously studied for flow control applications, the fan configuration was recently developed by Portugal et al. (2017) [44] to obtain uniform ozone distribution utilizing the SDBD flow generation mechanism and is yet to be studied for decontamination applications.

This research aims at the fundamental understanding of spatial and temporal distribution of surface DBD (SDBD) plasma generated ozone in air for effective decontamination. This includes (a)experimental investigation of effect of ozone distribution on decontamination, (b)comparison of ozone distribution produced by the fan and comb SDBD reactor experimentally and (c) simulation of ozone distribution by the two configurations.

II. Methods and Materials

This section is divided into 3 segments. The first segment describes the experimental set-up used to study the effect of better ozone distribution on decontamination efficacy. This is achieved with examination of overall decontamination of inoculated air with ozone produced by a comb SDBD reactor and distributed using an external fan. The second segment describes the experimental set up for studying and comparing ozone distribution by the Comb SDBD reactor and the novel fan SDBD reactor. The third segment talks about the numerical methods used in simulating flow and ozone distribution by the two SDBD reactor configurations.

A. Experimental set up 1: Effect of better ozone distribution on decontamination efficacy

Test organism: *Bacillus subtilis (B. subtilis)*, a gram-positive bacterium, is used as the test organism for testing the effect of ozone distribution on overall decontamination in an enclosed space. B. subtilis is a rod-shaped, spore forming aerobe generally found in soil and vegetation. This bacterial species is chosen as it is widely used for evaluating decontamination technologies in general and specifically for planetary protection studies [3]. Additionally, due to its spore forming ability, the inactivation of this species will also indicate the capability of DBD plasma sterilization.

Preparation of cultures: Frozen cultures of B. subtilis are stored at -80^{0}C in LB (Lysogeny Broth) broth with 30% glycerol. A sterile inoculating loop is swabbed with frozen cultures and streaked onto an LB plate. This plate is incubated at 37^{0}C for 24 hours to grow fresh cultures. Colonies from the fresh culture is then used to make up the LB broth culture with approximately 7 x10^4 CFU (colony forming units)/ml which is mixed with distilled de-ionized water to get contaminated water for aerosolizing.

DBD plasma generation: Figure 1 illustrates the comb electrode design and the corresponding power supply used in this study. In this configuration, plasmas are formed over the surface of the dielectric barrier and along the perimeter of the top electrode that is exposed to the surrounding air. Details of the reactor design, plasma generation and electrical power supply can be found in recently published works of our research group [45, 46].

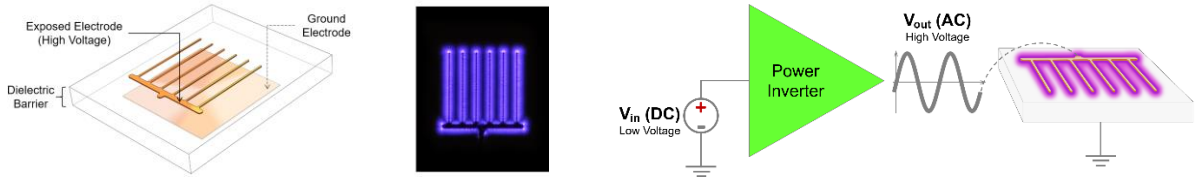

(a) (b) (c)

Fig. 1 Illustration of the Surface Dielectric Barrier Discharge (SDBD) comb-reactor. The image shows (a) a comb shaped SDBD plasma reactor showing the exposed and ground electrode separated by a dielectric of 0.76 mm thickness and 3.48 dielectric constant, (b) plasma formed around the exposed electrode when the reactor is powered and (c) the electrical power supply used to operate the SDBD plasma reactor [45].

The experimental set up used for this study is shown in Figure 2(a). The different components of the setup along with their functions are given in Table 1. A HYVAC PressoVac diaphragm vacuum pump (97000-001 PressoVac 24 Diaphragm Vacuum Pump [47]) with a maximum flow rate of 1 cu ft/min along with a flow control valve is used to control the air inflow rate into the test chamber. A Medneb compressor nebulizer MQ5600 [48] is used for inoculating the air volume inside the test chamber by aerosolizing contaminated water fed into the nebulizer cup. The aerosolized particles of 0.5-10 microns are sprayed into the test chamber at a flow rate of 0.18 LPM [48]. A bio-sampler (SKC Biostage single-stage Impactor), shown in Figure 2(b), is used for sampling the air inside the test chamber. The bio-sampler consists of an inlet cone, precision-drilled 400-hole impactor stage and a base which holds a standard-size agar plate. It is connected to a high flow pump (Quicktake 30) which pulls microorganisms in the sampled air at 14.5 LPM and collects them on the agar surface through the holes in the impactor stage [49].

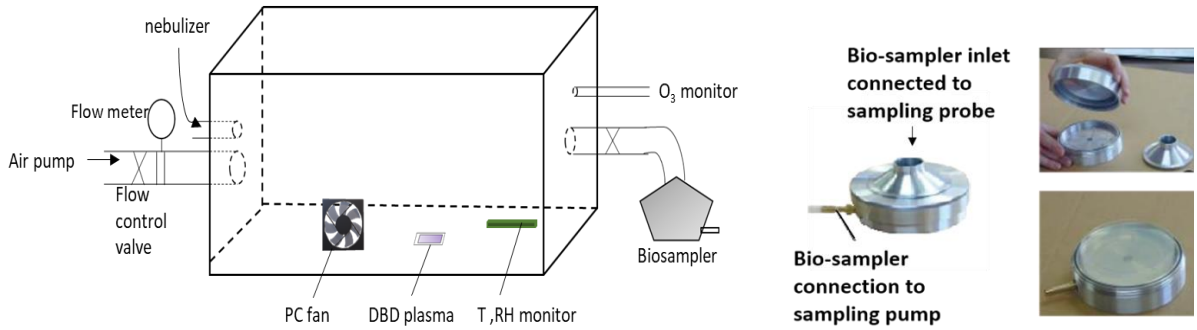

(a) (b)

Fig. 2 Illustration of the (a)experimental set up used for studying effect of ozone distribution on decontamination and (b) biosampler (SKC Biostage single-stage Impactor) used to sample air.

Table 1 Components of experimental set up and their functions

Sr No.	Component	Function
1	Air pump + valve +flow meter	Control the inflow air rate to the chamber
2	Nebulizer	Inoculate the air inside the test chamber
3	Plasma Reactor	Produce ozone and decontaminate the air
4	CPU Fan	Distribute the ozone produced inside the chamber
5	Ozone monitor	Monitor the ozone levels inside the chamber
6	Biostage sampler +valve + pump	Sample air to quantify decontamination
7	Temperature and humidity chart recorder EXTECH Instruments RH520A-NIST	Measure temp and relative humidity

Procedure: In the beginning of every experiment, the test chamber and all the components inside it are sterilized with 70% isopropyl alcohol to avoid external contamination. Further, before starting any experiment, ozone levels inside the test chamber are measured to be in stable levels of 20-30 ppb. This is ensured by letting the ozone monitor run for 20 to 30 minutes without closing the chamber lid or the valves. The room ozone levels measured fall in the range of ozone levels reported in buildings and laboratories without ozone sources [49]. Two sets of experiments are performed – (a) with and (b) without the external fan used for ozone distribution. The external fan is used for ozone distribution as the comb SDBD plasma reactor configuration has been shown to not uniformly distribute ozone and instead drives away the generated ozone as wall jets parallel to the reactor surface [44]. This occurs due to the nature of the flow induced by the comb configuration as shown in Figure 5.

The first set of experiments are performed without using the fan for ozone distribution. At first, 0.1 ml of the LB broth culture is used to inoculate 50 ml of distilled DI water. The contaminated water is then fed into the nebulizer cup. The nebulizer is switched on for 6 seconds to inoculate the air in the test chamber. The nebulizer run time of 6 seconds is determined from initial runs to obtain a consistent initial bacterial count of approximately $2x10^3$ CFUs in the inoculated volume. Following aerosolization with the nebulizer, the air is sampled using the biostage impacter to get the control bacterial count. During the air sampling, the air pump is switched on and the valve connecting the pump to the test chamber is adjusted to equate the inflow rate to the flow rate of air being sampled to avoid change in air pressure inside the chamber. Once the air is sampled, both the valves at the inlet and outlet of the test chamber are closed and the plasma reactor is run for 10 minutes. At the end of 10 mins, the air is sampled again using the biostage sampler.

Post experimental procedure: Every time air is sampled, agar plates are taken out of the bio-stage sampler and incubated at 37^0C for 24 hours. Plate counts are obtained from the agar plates to quantify the bacterial colonies present

in the sampled air. The plate counts along with the total volume of the chamber (0.07 m^3) and the sampled air volume (0.007m^3) are used to calculate the total CFUs present in the test chamber before and after plasma treatment. The distribution of the aerosolized bacteria is assumed to be uniform in the inoculated volume for these calculations. Following each experimental run, the residual ozone inside the test chamber is removed using a vacuum cleaner till ozone levels reach room levels of below 30 ppb. The test chamber and the components inside it are then cleaned with 10% sodium hypochlorite solution, left to stand for 30 minutes and wiped with 70% alcohol before starting another experiment. Additionally, before refilling the nebulizer cup when required, it is sterilized with 10% sodium hypochlorite solution and wiped with 70% alcohol to avoid inconsistent bacterial count in the inoculated air volume. The same procedure is followed to run the second set of experiments which employs a fan for distribution of plasma generated ozone in addition to the other components used in the first set of experiments.

Control experiments: Air inside the test chamber is sampled before every experiment to check for external bacterial contamination that may be present. Ozone levels are monitored inside the test chamber with free airflow at the inlet for 20 minutes before each experiment to ensure room levels of ozone (20-30 ppb) [49] inside the test chamber.

B. Experimental set up 2: Comparison of ozone distribution by Comb and Fan SDBD reactor

This set up is used to study the temporal and spatial distribution of ozone in an enclosed space with the Comb and Fan SDBD plasma reactor configurations. With the recently developed fan configuration [44] with better flow distribution ability, this experimental study was done to compare the ozone distribution by the comb and fan configurations.

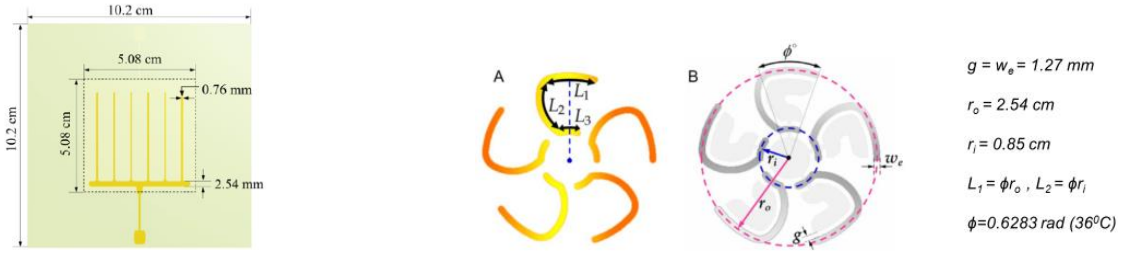

(a) (b)

Fig. 3 (a) Comb reactor configuration and (b) Fan reactor configuration. [44]

DBD plasma generation: Figure 3 illustrates the electrode design and dimensions used for the study of temporal and spatial distribution of ozone produced by the comb and fan design configuration of the SDBD plasma reactor. Material properties of the dielectric material and the electrodes are same as the one used in Experimental set up 1. Input voltage (25 V) for the plasma reactors in these experiments is supplied by a function generator. The function generator generates an RF sine wave signal which is then passed through a power amplifier. The amplified signal then passes through a step-up transformer which steps up the voltage. The input power from the transformer is used to power the plasma reactor.

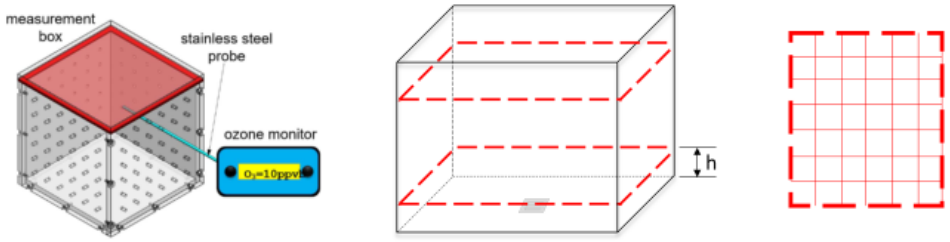

(a) (b) (c)

Fig. 4 Illustration of (a) the experimental test chamber used to measure ozone distribution produced by two SDBD plasma reactor configurations, (b) planes of measurements that are defined by their vertical distance from the surface of the plasma reactor and (c) grid of measurement points at each plane.

The experimental set up for collecting spatial and temporal ozone distribution data mainly consists of a polycarbonate test chamber with internal dimensions of 27.3 cm x 27.3 cm x 28.6 cm, a plasma reactor(comb/fan) and an ozone monitor as shown in Figure 4(a). The 2B Technologies Model 202 Ozone Monitor™, which works based on UV light absorption at 254 nm, is used for the ozone measurements in air. The accuracy of the monitor is 1.5 ppb or 2% of the reading [51]. Each wall of the chamber has 36 holes of 0.7 cm diameter for insertion of a stainless-steel ozone probe connected to the ozone monitor. Measurements are made at a number of points in planes at different heights from the bottom of the chamber as shown in Figure 4(b). Each measurement plane has measurement points at intersection of the grid lines as shown in Figure 4(c). The grid point measurements are obtained by placing the ozone probe at different points with the help of the holes in the chamber walls. At least 3 measurements are taken at each point to minimize errors. Polycarbonate material and stainless-steel materials are chosen for the chamber and the probe as they are known to be resistant to reactions with ozone. The test chamber is sealed with a silicon layer to avoid ozone leakage from the test chamber. Ozone measurements are obtained for 5 minutes from the time when the plasma reactor is switched on. After each experimental run of 5 minutes, the plasma reactor is turned off. Following this, the residual ozone is removed with a vacuum cleaner till ozone levels reach room levels of around 20-30 ppb [50]. Before starting each experimental run, the test chamber is let to stand with the lid open and ozone levels are monitored inside it for 15 minutes to reduce error in ozone measurements.

C. Numerical set up: Comparison of ozone distribution by Comb and Fan reactor

Numerical simulation of the ozone distribution generated by the fan and comb plasma reactor configurations is carried out in two stages: airflow simulations and airflow incorporated with ozone source and decomposition. The flow simulations are run using ANSYS FLUENT [52]. The basic governing equations (continuity, momentum and energy equations) along with a body force model corresponding to the SDBD plasma reactor force generation are used for the flow simulations.

Body Force Model: The body force model used in this study is obtained from the study performed by Singh and Roy [53] on simulating effects of plasma actuators. A similar body distribution function is applied in this study for modeling the body force distribution functions for the comb and fan reactor. It is given by:

$$F_{\varsigma} = \frac{F_{\varsigma o}}{\sqrt{{F_{\varsigma o}}^2 + {F_{y o}}^2}} exp\left\{-\left[\frac{(\varsigma-\varsigma_o)-(y-y_o)}{y-y_o+y_b}\right]^2 - \beta_{\varsigma}(y-y_o)^2\right\}; F_y = \frac{F_{y o}}{\sqrt{{F_{\varsigma o}}^2 + {F_{y o}}^2}} exp\left\{-\left[\frac{(\varsigma-\varsigma_o)}{y-y_o+y_b}\right]^2 - \beta_y(y-y_o)^2\right\}$$

where $F_{\varsigma_o} = 2.6, F_{y_o} = 2.0, \beta_{\varsigma} = 1.44x105, \beta_y = 1.8\ x\ 106, y_b = 0.001665$ while ς_o and y_o give the location of the actuation corresponding to the points along the lines of actuation (e.g., along the edge of the exposed electrode)of the specific SDBD plasma configuration[54].

The lines of actuation for modeling the body force distribution of the comb SDBD reactor are shown in Figure 5(b). Flow induced by the comb configuration is shown in Figure 5(c).

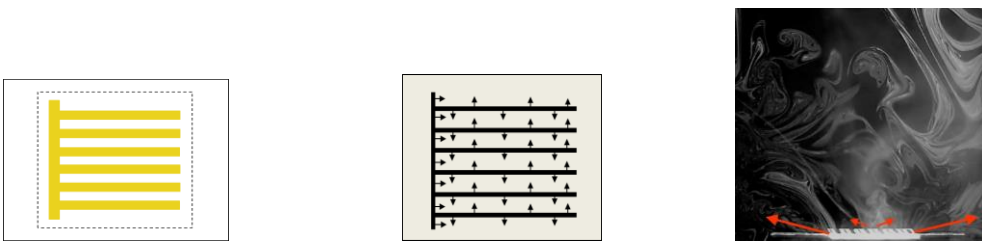

(a) (b) (c)

Fig. 5 Illustration of (a) the exposed (yellow) and ground (dotted) electrodes of the SDBD comb reactor used for modeling ozone distribution and (b) corresponding lines of actuation and force distribution used in body force distribution modeling (c) Smoke flow visualization of flow generated by the comb SDBD reactor showing plasma induced flow [44].

The lines of actuation for the fan reactor configuration is shown in Figure 6(b). Each blade of the fan configuration has four lines of actuations- L1, L2, L3 and L4 as shown in Figure 6(b).

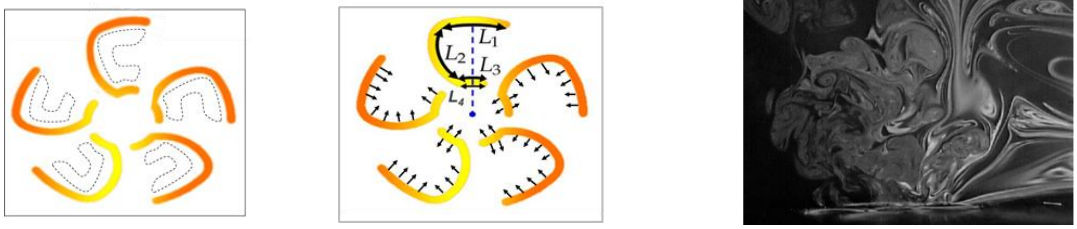

(a) (b) (c)

Fig. 6 Illustration of (a) the exposed (yellow) and ground (dotted) electrodes of the SDBD fan reactor used for modeling ozone distribution, (b) lines of actuation and force distribution used in body force distribution modeling and (c) smoke flow visualization of the flow generated by the fan configuration [44].

The combination of forces induced by the 5 blades and the center arc of the fan reactor (Figure 6(b)) result in suction of the air near the electrode perimeter followed by ejection leading to the formation of vortical structures indicating turbulence. Thus, turbulence modelling is considered for modelling flow generated by the fan DBD reactor configuration.

Ozone distribution is obtained by solving a species transport equation with ozone source and experimentally documented ozone decomposition reaction rates by SDBD reactors [46]. Simulation of ozone distribution generated by the reactor configurations is performed by taking convection, diffusion, ozone generation rate and ozone decay rates (from previous experimental data [46]).

III. Results and discussion

A. Experimental data 1: Effect of better ozone distribution on decontamination efficacy.

Control experiments: Air inside the test chamber sampled before running the experiments indicated undetectable levels of culturable bacterial concentration. These measurements were taken prior to starting every experiment. Ozone levels monitored inside the test chamber before each experiment for 20 minutes indicated ozone concentrations of room level (20-30 ppb) [49]. This was expected as measures were taken to eliminate any residual ozone from previous experiments.

Temperature inside the chamber remained at 23±2 deg Celsius for all the experiments. The relative humidity levels varied between 73% to 78%. The variations in the relative humidity inside the chamber can be explained by the nebulizer aerosolization. However, since the nebulizer was switched on only for 6 seconds, it did not vary the relative humidity inside the chamber by significant amounts.

As explained in the methods section, two sets of experiments were performed. The first set of experiments did not involve using the external fan for ozone distribution inside the chamber. The contaminated air inside the test chamber was exposed to plasma for 10 minutes for these experiments. Air was sampled before and after plasma exposure to obtain the resulting disinfection. The disinfection results are provided in Tables 2 and 3.

Table 2: Bacterial concentrations inside the test chamber before and after plasma treatment for 10 minutes.

Experiment number	Bacterial concentration before plasma exposure (CFUs)	Bacterial concentration after plasma exposure (CFUs)	Percentage reduction (%)
1	$1.2\text{x}10^3$	$2.6\text{x}10^2$	77.7
2	$2.1\text{x}10^3$	$6.4\text{x}10^2$	69.5
3	$2.7\text{x}10^3$	$7.1\text{x}10^2$	74.1
4	$2.4\text{x}10^3$	$4.8\text{x}10^2$	79.8
5	$8.1\text{x}10^2$	$1.0\text{x}10^2$	86.8

Table 3: Bacterial concentrations measured inside the test chamber equipped with an external fan for ozone distribution before and after plasma treatment for 10 minutes.

Experiment number	Bacterial concentration before plasma exposure (CFUs)	Bacterial concentration after plasma exposure (CFUs)	Percentage reduction (%)
1	$2.4x10^3$	$8.7x10^1$	96.5
2	$1.9x10^3$	$1.8x10^1$	99.0
3	$3.0x10^3$	$7.7x10^1$	97.4
4	$1.5x10^3$	$1.5x10^1$	98.8
5	$1.7x10^3$	$2.8x10^1$	98.3

An average percentage reduction of 77.6% was observed in the bacterial concentrations measured before and after plasma treatment in the first set of experiments conducted without using the external fan for ozone distribution. 98% average percentage reduction was obtained when an external fan was used for distribution of ozone formed by the plasma reactor in the second set of experiments.

These results imply significant reduction (~78%) in bacterial concentrations in air using the DBD plasma reactor and suggest that more effective disinfection (~98%) can be obtained when the plasma-generated ozone is distributed in the contaminated volume of air. It is to be noted here that we use percentage reduction in place of common log reduction count since initial microbial concentrations in air are kept low following general trends of air contamination observed [55]. The experimental investigation of effect of ozone distribution on decontamination suggests enhanced decontamination with better ozone distribution.

B. Experimental data 2: Comparison of ozone distribution by Comb and Fan reactor

Ozone measurements were taken in the polycarbonate chamber as described in the experimental procedure to take measurements in 2 planes for 5 minutes after the reactor was powered up. The two planes P1 and P2 (Figure 7(a)) were located at 3.5 and 11.5 from the SDBD plasma reactor surface placed at the center of the bottom surface of the test chamber, respectively.

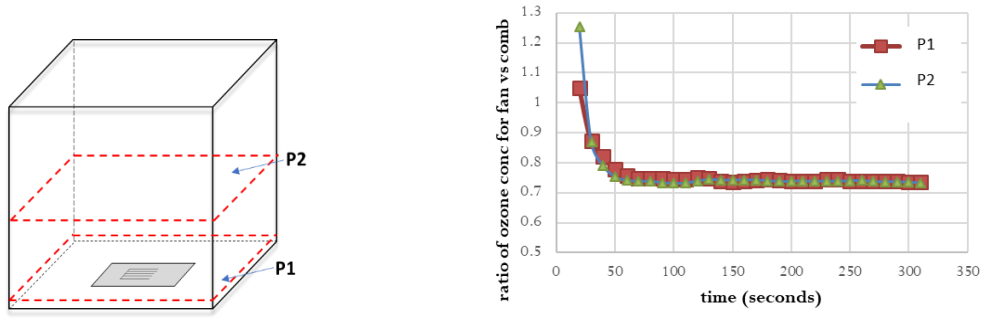

(a) (b)

Fig. 7 (a) Experimental set up used to measure ozone concentrations at different points inside the test chamber and (b) ratio of ozone concentrations for fan and comb reactors averaged over planes P1 and P2.

It was observed that the fan SDBD reactor had slightly less overall ozone concentrations at different measurement points when compared to the comb reactor. Inspection of the ozone concentrations obtained for the two reactor configurations led to an interesting observation which was used to get comb-equivalent concentrations for the fan reactor at each grid point. The ratio of ozone concentrations at each grid point for the fan reactor and the comb reactor was found to be fairly constant at 0.76 for P1 and P2. Figure 7(b) shows the ratio of ozone

concentrations for fan and comb configurations averaged for different points in a plane at each time point. The constant ratio for the ozone concentration values of the fan and comb configuration was used to calculate comb-equivalent fan ozone concentration values at each grid point. These concentrations were compared to ozone concentrations corresponding to the comb configuration for each plane.

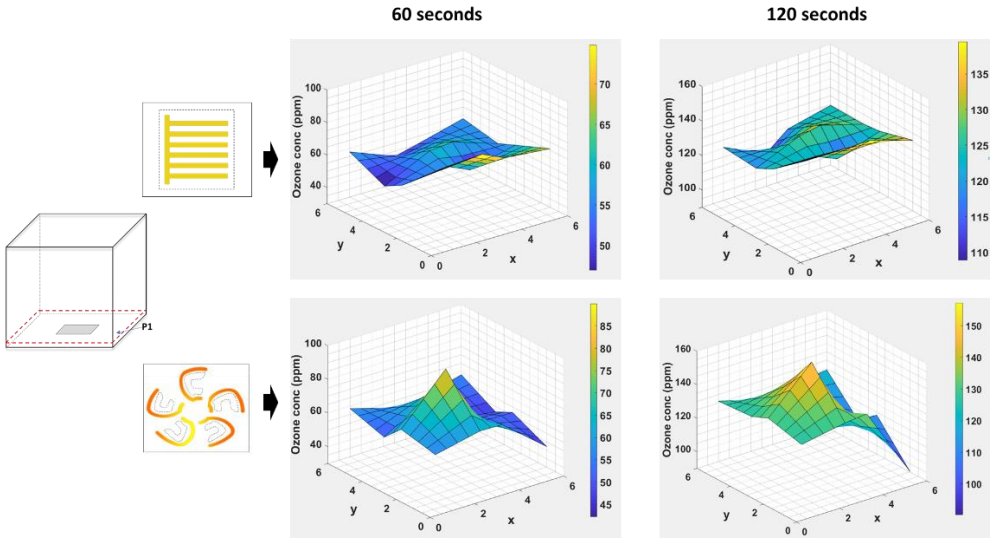

(a) (b)

Fig. 8 Ozone concentration for comb configuration and equivalent ozone conc for fan configuration (a) in plane P1 and (b) plane 2 at 60 seconds and 120 seconds; units: ppm.

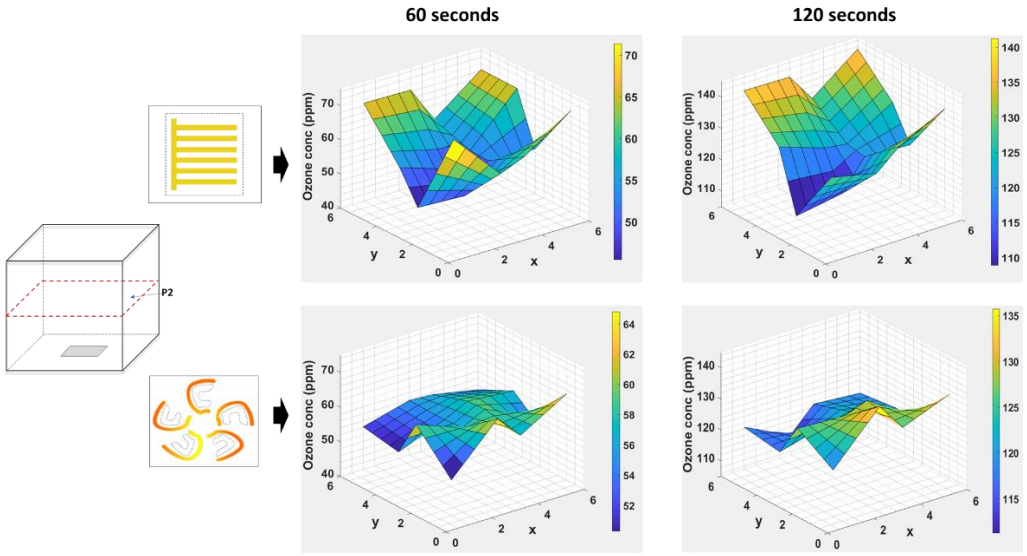

(a) (b)

Fig. 9 Ozone concentration for comb configuration and equivalent ozone conc for fan configuration (a) in plane P1 and (b) plane 2 at 60 seconds and 120 seconds; units: ppm.

Figure 8 shows the ozone distribution obtained in P1 at 1 and 2 minutes for the two reactor configurations. Since plane 1 is very close to the actuator surface, the ozone distribution observed in this plane demonstrates the evolution of ozone concentrations near the actuator surface. The ozone concentrations for the fan reactor follow the corresponding flow pattern with ozone formation at the center and distributed through the plane with time. For the

comb reactor, ozone formed near the actuator surface is carried with the wall jet in a direction towards one of the chamber walls.

Figure 9 shows the ozone distribution obtained in P2 at 1 and 2 minutes. Since P2 is away from the bottom or top chamber wall the distribution obtained here is a better indication of the differences in ozone distribution due to the two reactor configurations. It is observed here that the comb configuration results in a biased distribution of ozone with higher concentrations towards one chamber wall. In comparison, the fan configuration results in a fairly even distribution through the plane. The uniform ozone distribution observed in this plane with the fan configuration indicates that much better ozone distribution is achieved with the fan configuration in comparison to the comb configuration.

C. Simulation data: Comparison of ozone distribution by Comb and Fan reactor

For simulating the ozone distribution inside a chamber resulting from the comb and fan reactor configuration, the flow distribution of the configurations was simulated followed by inclusion of ozone generation and distribution. All the simulations were performed using ANSYS FLUENT. The chamber dimensions used in the simulations were chosen as that of the polycarbonate chamber used in experimental set up 2 and 3 for matching the simulated ozone distribution results to experimental ozone distribution and disinfection distribution.

For these simulations, the flow and ozone distribution were simulated in a three-dimensional box of size [0, 0.273 m] x [0, 0.273 m] x [0, 0.286 m] in the x, y, z directions. 452829 grid points was used to resolve the mesh for the flow simulations. The mesh was highly refined at the reactor surfaces and 3 cm in each direction around it. The walls of the chamber are kept at zero flux along with no slip boundary condition. The flow is initialized with very low velocities of 10^{-5} m/s to resemble quiescent conditions. For the ozone distribution simulations three species: Oxygen, Ozone and Nitrogen are considered with initial mixture fractions of 0.23, 0 and 0.77, respectively. A source term for ozone 1.8 x 10 $^{-8}$ kg/m^3-s is applied in the cells over the actuator surface based on experimental ozone concentration measurements. An equivalent sink term for oxygen is applied for mass conservation inside the chamber. A first order ozone decomposition is also included in the form for Arrhenius rate equation. The Activation energy and pre-exponential factor in the Arrhenius rate equation was obtained by matching it with experimental ozone decomposition equation obtained by Portugal et al. [46]. Finite rate model was used for the ozone decomposition reactions.

Comb and Fan flow results: The dimensions of the comb and fan SDBD reactor used for simulating the flow fields were matched to that used by Portugal et al. [44] for experimental study of the comb and fan flow induction using PIV (particle image velocimetry). The simulated results are compared to experimental comb flow distribution obtained by Portugal et al. [44] as shown in Figure 12 to 15.

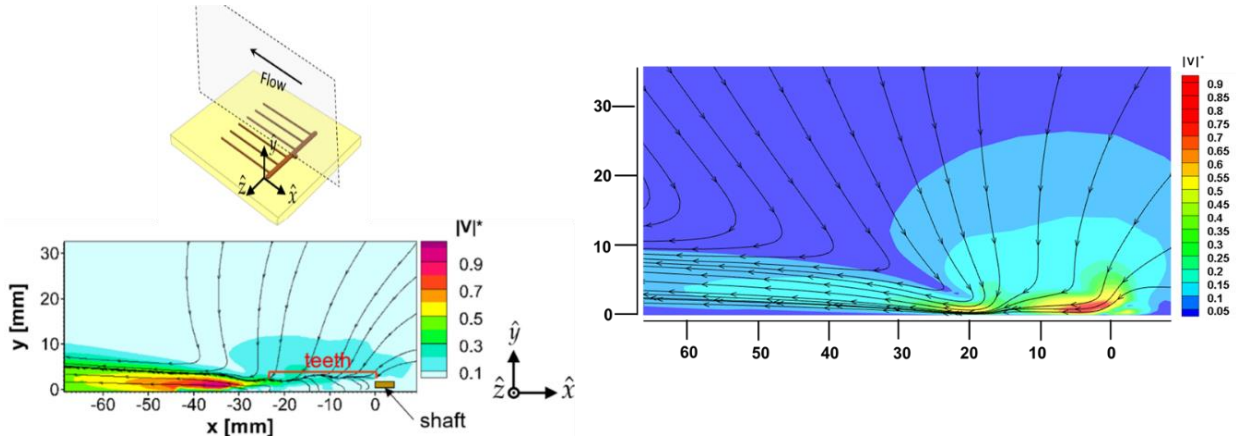

Fig. 12 Illustration of (a) Plane of view along the teeth of the comb SDBD reactor, (b) Experimental flow distribution [44] and (c) Simulated flow distribution.

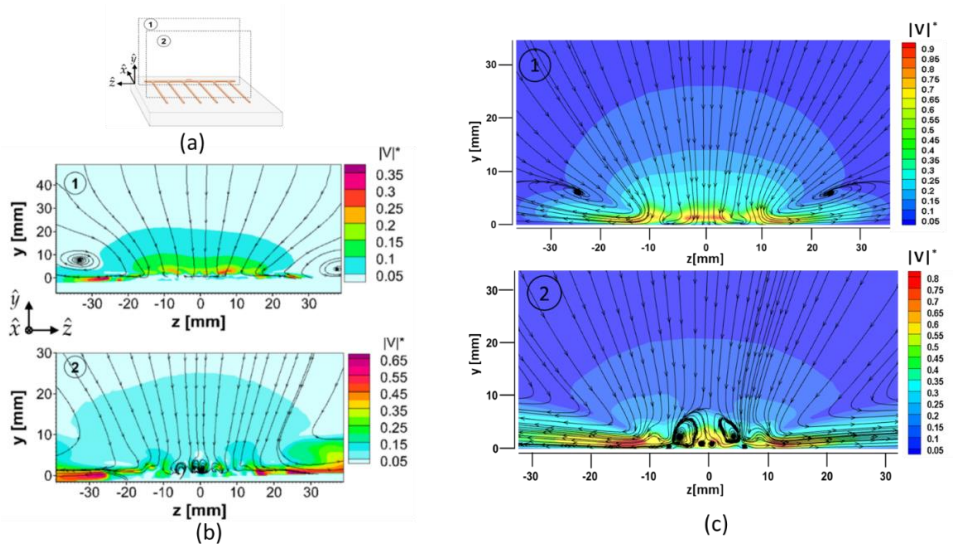

Fig. 13 Illustration of (a) Plane of view across the teeth of the comb SDBD reactor, (b) Experimental flow fields showing normalized velocity magnitudes [44] and (c) Simulated flow fields with normalized velocity magnitudes.

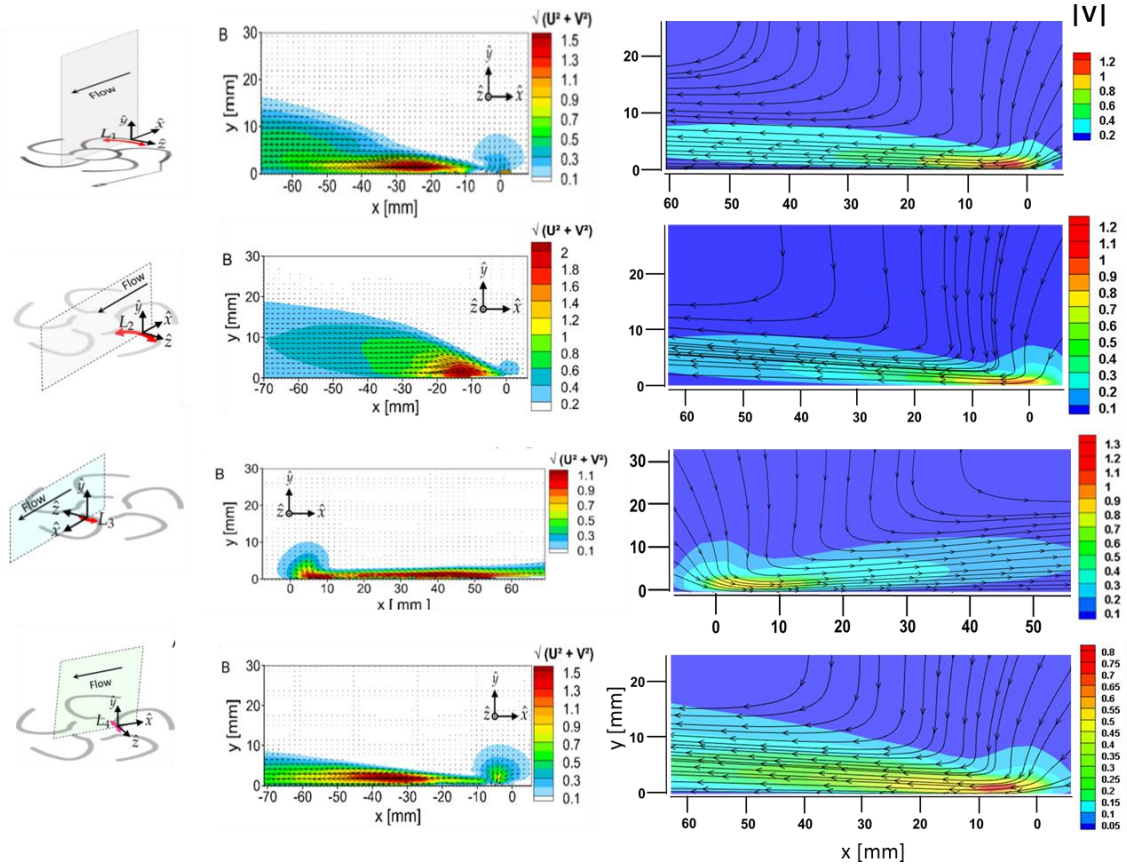

(a) (b) (c)

Fig. 14 Illustration of (a) Planes of views for four lines of 1 blade of the fan SDBD reactor [44], (b) Experimental flow fields for each separate line: L1, L2, L3, L4 [44] and (c) Corresponding simulated flow fields.

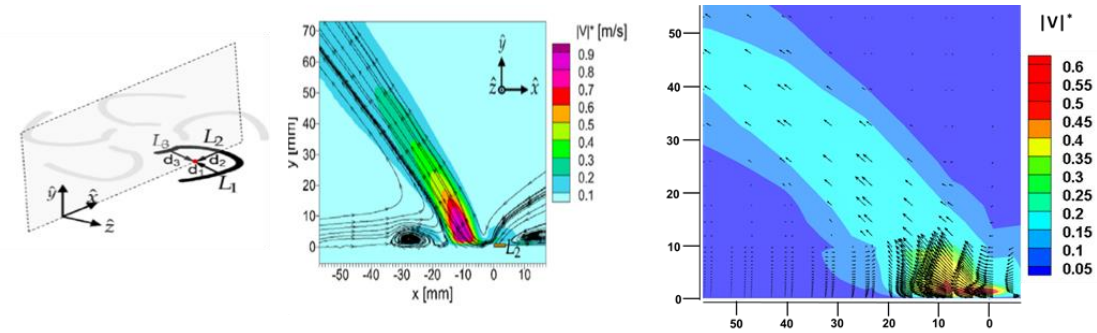

(a) (b) (c)

Fig. 15 Illustration of (a) Plane of views for 1 blade of the fan SDBD reactor [44], (b) Experimental flow field [44] and (c) Simulated flow fields for 1 blade of the Fan SDBD reactor.

The simulated flow fields qualitatively match well with the previously published experimental data [44] as shown in Figure 12-15. However, higher velocity magnitudes are observed near the SDBD reactor surface in the simulated results compared to experimental data. These discrepancies between simulated and experimental data near the SDBD reactor surface can be attributed to error in PIV (particle image velocimetry) experimental data near the area of plasma formation due to interaction of seeding oil particles with high electric fields near the electrode surfaces. This phenomenon has been studied by A. Masati et. al [56] and M. Hamdi et. al [57] where the effect of electric fields near the plasma formation area result in oil seeding particles flowing from the ground to exposed electrode in contrast to the atmospheric flow field from the exposed to the ground electrode. This results in lower velocities to be observed near the plasma surface than the actual velocities of the induced flow field.

Ozone distribution results: Ozone distribution produced by the two reactor configurations were simulated. The dimensions of the comb and fan reactor used for these simulations were same as the ones used in experimental study of ozone distribution described previously. The simulated results of normalized ozone distribution produced in the chamber at 10 seconds after powering up the SDBD reactors are shown in Figure 16 and 17.

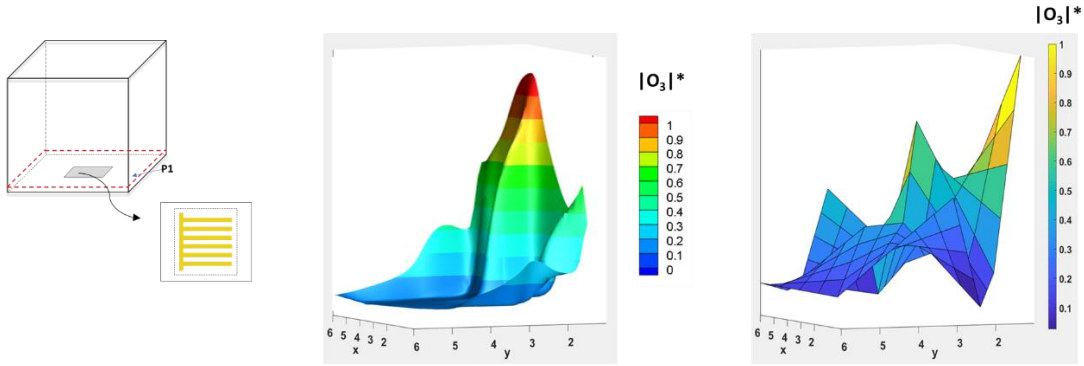

(a) (b) (c)

Fig. 16 (a) Plane of observation (P1) and comb SDBD reactor configuration, (b)simulated results of ozone distribution observed in P1 at 10 seconds of powering up the reactor inside the test chamber and (c) corresponding experimental ozone distribution results at 10 seconds.

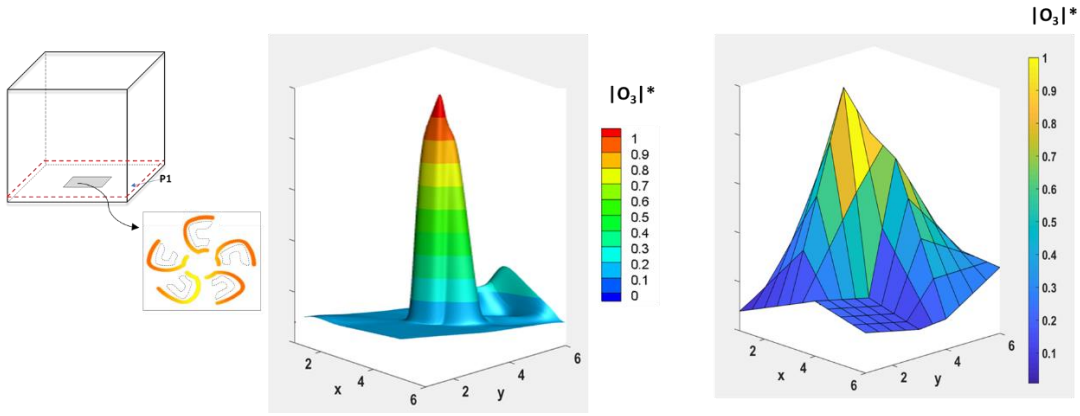

(a) (b) (c)

Fig. 17 (a) Plane of observation (P1) and Fan SDBD reactor configuration, (b)simulated results of ozone distribution observed in P1 at 10 seconds of powering up the reactor inside the test chamber and (c) corresponding experimental ozone distribution results at 10 seconds.

The simulated results fairly match with the experimental distribution obtained. Figure 15 shows higher concentrations near one wall of the chamber resulting from the wall jet produced by the comb SDBD reactor. In comparison, Figure 16 shows the initial distribution of ozone by the fan SDB reactor with higher concentrations at the center to be distributed evenly through the chamber with time. The simulated ozone distribution at 10 seconds of powering up the reactors results indicate the pathway to obtaining the ozone distribution data observed experimentally for 60 and 120 seconds previously shown in Figure 8 and 9.

Ozone generated near the reactor surface for the comb reactor is pushed towards the direction of the teeth tips as observed in the experimental data. For the fan reactor, the ozone generated is distributed from the center towards the 4 walls similar to the experiments. Thus, the simulated data represents the trends of ozone generated and suggests how the ozone would be distributed depending on the electrode configurations of the SDBD reactors. However, for exact comparison of ozone concentrations in different planes at different times inside the chamber, a more extensive study will be performed in the future.

IV. Conclusion

This paper demonstrates enhanced decontamination with better distribution of SDBD plasma generated ozone and evaluates the comb and fan reactor configurations for ozone distribution resulting from flow actuation. Experimental investigation of the effect of ozone distribution on decontamination using an external fan along with a comb plasma reactor showed a 20% increase in percentage reduction of bacterial count in an enclosed volume suggesting better decontamination with better ozone distribution. Thus, flow actuation characteristics of plasma reactors commonly used in aerodynamic flow control can be employed to improve the distribution of the generated ozone resulting in lower ozone requirements and energy consumption. Thus, for decontamination applications like sterilization of spacecraft components, ozone distribution resulting from inherent flow actuation of plasma reactors instead of using an external distribution source would be advantageous. To study the effect of flow inducement on distribution of ozone produced during plasma generation two configurations: the comb and fan SDBD reactors were simulated and examined experimentally. Experimental results showed a biased ozone distribution in one direction of the test chamber when the comb plasma reactor was used. This was expected as the flow actuation resulting from the comb configuration is known to produce a wall jet parallel to the reactor surface and in the direction of the comb tips. In contrast, the recently developed fan plasma reactor showed a more uniform distribution where the ozone generated was radially distributed from the center in all directions from the reactor. This corresponds well with previously studied flow actuation characteristics of the fan configuration which produces vortical structures near the surface spreading radially outward and upward from the center of the fan. The fan plasma reactor proved to be a better ozone distributer with uniform non-biased distribution compared to the comb reactor where maximum ozone concentrations were pushed towards one side of the test chamber. This implies that the fan configuration would be better for decontamination applications due to enhanced and uniform ozone distribution. Flow fields by the comb and fan

reactor, up till 10 seconds of powering up the reactor, were also simulated and validated with experimental data. The peaks of ozone concentrations observed for the comb configuration were observed near the wall in the direction of the comb tips. In contrast, the peaks of ozone concentrations for the fan configuration were found at the center of the chamber with fairly uniform radial gradients. Thus, the simulated results further confirm the ability of fan SDBD reactors to uniformly distribute ozone in an enclosed space and hence, their suitability for decontamination applications. Thus, this study showed more effective decontamination with better ozone distribution and the ability of the recently developed fan plasma reactor configuration to uniformly distribute ozone for the same purpose. Further, simulation studies of ozone distribution by SDBD plasma reactors can help in designing optimum reactor configurations for efficient decontamination in applications like sterilization of spacecraft components and bio-clean rooms.

References

[1] Kminek G, Conley C, Hipkin V, Yano H. COSPAR's planetary protection policy. Space Research Today. 2017. 200, 12–25.

[2] Stieglmeier M, Rettberg P, Barczyk S, Bohmeier M, Pukall R, Wirth R, Moissl-Eichinger C. Abundance and diversity of microbial inhabitants in European spacecraft-associated clean rooms. Astrobiology. 2012 Jul 1;12(6):572-85.

[3] Shimizu S, Barczyk S, Rettberg P, Shimizu T, Klaempfl T, Zimmermann JL, Hoeschen T, Linsmeier C, Weber P, Morfill GE, Thomas HM. Cold atmospheric plasma–A new technology for spacecraft component decontamination. Planetary and Space Science. 2014 Jan 1;90:60-71.

[4] Bashir, M., Ahmed, M., Weinmaier, T., Ciobanu, D., Ivanova, N., Pieber, T. R., & Vaishampayan, P. A. (2016). Functional metagenomics of spacecraft assembly cleanrooms: presence of virulence factors associated with human pathogens. Frontiers in microbiology, 7, 1321.

[5] European Cooperation for Space Standardization, "ECSS-Q-ST-70-56C vapour phase bioburden reduction for flight hardware," ECSS (2013).

[6] European Cooperation for Space Standardization, "ECSS-Q-ST-70-57C dry heat bioburden reduction for flight hardware" (2013).

[7] Office of Planetary Protection, National Aeronautics and Space Administration "Mission Requirements" [online database](2019), URL: https://planetaryprotection.nasa.gov/requirements

[8] European Cooperation for Space Standardization, "ECSS-Q-ST-70-53C materials and hardware compatibility tests for sterilization processes" (2008).

[9] Shimizu T, Zimmermann JL, Morfill GE. The bactericidal effect of surface micro-discharge plasma under different ambient conditions. New Journal of Physics. 2011 Feb 11;13(2):023026.

[10] Lerouge S, Wertheimer MR, L'H Y. Plasma sterilization: a review of parameters, mechanisms, and limitations. Plasmas and Polymers. 2001 Sep 1;6(3):175-88.

[11] Laroussi M. Sterilization of contaminated matter with an atmospheric pressure plasma. IEEE Transactions on Plasma Science. 1996 Jun;24(3):1188-91.

[12] Schuerger AC, Trigwell S, Calle CI. Use of non-thermal atmospheric plasmas to reduce the viability of Bacillus subtilis on spacecraft surfaces. International Journal of Astrobiology. 2008 Jan;7(1):47-57.

[13] Cooper M. Elucidation of Levels of Bacterial Viability Post-Non-Equilibrium Dielectric Barrier Discharge Plasma Treatment (Doctoral dissertation, Drexel University).

[14] De Geyter N, Morent R. Nonthermal plasma sterilization of living and nonliving surfaces. Annual review of biomedical engineering. 2012 Aug 15;14:255-74.

[15] Moreau M, Orange N, Feuilloley MG. Non-thermal plasma technologies: new tools for bio-decontamination. Biotechnology advances. 2008 Nov 1;26(6):610-7.

[16] Moisan M, Barbeau J, Crevier MC, Pelletier J, Philip N, Saoudi B. Plasma sterilization. Methods and mechanisms. Pure and applied chemistry. 2002 Jan 1;74(3):349-58.

[17] Park GY, Park SJ, Choi MY, Koo IG, Byun JH, Hong JW, Sim JY, Collins GJ, Lee JK. Atmospheric-pressure plasma sources for biomedical applications. Plasma Sources Science and Technology. 2012 Jun 6;21(4):043001.

[18] Graves DB. The emerging role of reactive oxygen and nitrogen species in redox biology and some implications for plasma applications to medicine and biology. Journal of Physics D: Applied Physics. 2012 Jun 13;45(26):263001.

[19] Gazeli K, Noel C, Clément F, Daugé C, Svarnas P, Belmonte T. A study of helium atmospheric-pressure guided streamers for potential biological applications. Plasma sources science and technology. 2013 Apr 2;22(2):025020.

[20] Kim GC, Lee HW, Byun JH, Chung J, Jeon YC, Lee JK. Dental applications of low-temperature nonthermal plasmas. Plasma Processes and Polymers. 2013 Mar;10(3):199-206.

[21] Barekzi N, Laroussi M. Dose-dependent killing of leukemia cells by low-temperature plasma. Journal of Physics D: Applied Physics. 2012 Oct 4;45(42):422002.

[22] Dawson R, Little J. Characterization of nanosecond pulse driven dielectric barrier discharge plasma actuators for aerodynamic flow control. Journal of Applied Physics. 2013 Mar 14;113(10):103302.

[23] Corke TC, Post ML, Orlov DM. SDBD plasma enhanced aerodynamics: concepts, optimization and applications. Progress in Aerospace Sciences. 2007 Oct 1;43(7-8):193-217.

[24] Moreau E. Airflow control by non-thermal plasma actuators. Journal of physics D: applied physics. 2007 Jan 19;40(3):605.

[25] Bahri M, Haghighat F, Rohani S, Kazemian H. Impact of design parameters on the performance of non-thermal plasma air purification system. Chemical Engineering Journal. 2016 Oct 15;302:204-12.
[26] Schmid S, Jecklin MC, Zenobi R. Degradation of volatile organic compounds in a non-thermal plasma air purifier. Chemosphere. 2010 Mar 1;79(2):124-30.
[27] Gallagher MJ, Gutsol A, Friedman G, Fridman A. Non-thermal plasma applications in air-sterilization. In17th International Symposium on Plasma Chemistry, Toronto, Canada 2005 Aug 7 (pp. 1056-1057).
[28] Kamgang-Youbi G, Herry JM, Meylheuc T, Brisset JL, Bellon-Fontaine MN, Doubla A, Naïtali M. Microbial inactivation using plasma-activated water obtained by gliding electric discharges. Letters in applied microbiology. 2009 Jan;48(1):13-8.
[29] Machala Z, Hensel K, Akishev Y, editors. Plasma for bio-decontamination, medicine and food security. Springer Science & Business Media; 2012 Feb 5.
[30] Misra NN, Tiwari BK, Raghavarao KS, Cullen PJ. Nonthermal plasma inactivation of food-borne pathogens. Food Engineering Reviews. 2011 Dec 1;3(3-4):159-70.
[31] Surowsky B, Schlüter O, Knorr D. Interactions of non-thermal atmospheric pressure plasma with solid and liquid food systems: a review. Food Engineering Reviews. 2015 Jun 1;7(2):82-108.
[32] Scholtz V, Pazlarova J, Souskova H, Khun J, Julak J. Nonthermal plasma—a tool for decontamination and disinfection. Biotechnology advances. 2015 Nov 1;33(6):1108-19.
[33] Cooper M, Fridman G, Staack D, Gutsol AF, Vasilets VN, Anandan S, Cho YI, Fridman A, Tsapin A. Decontamination of surfaces from extremophile organisms using nonthermal atmospheric-pressure plasmas. IEEE transactions on plasma science. 2009 Jun;37(6):866-71.
[34] Hamajima S, Kawamura N, Nagatsu M. Low-Temperature Disinfection of Tea Powders Using Non-equilibrium Atmospheric Pressure Plasma. InRecent Global Research and Education: Technological Challenges 2017 (pp. 269-275). Springer, Cham.
[35] Laroussi M, Leipold F. Evaluation of the roles of reactive species, heat, and UV radiation in the inactivation of bacterial cells by air plasmas at atmospheric pressure. International Journal of Mass Spectrometry. 2004 Apr 15;233(1-3):81-6.
[36] Mastanaiah N, Banerjee P, Johnson JA, Roy S. Examining the role of ozone in surface plasma sterilization using dielectric barrier discharge (DBD) plasma. Plasma Processes and Polymers. 2013 Dec;10(12):1120-33.
[37] Efremov NM, Adamiak BY, Blouchin VI, Dadashev SJ, Dmitriev KJ, Gryaznova OP, Jusbashev VF. Action of a self-sustained glow discharge in atmospheric pressure air on biological objects. IEEE Transactions on plasma science. 2000 Feb;28(1):238-41.
[38] Schwabedissen A, Łaciński P, Chen X, Engemann J. PlasmaLabel–a new method to disinfect goods inside a closed package using dielectric barrier discharges. Contributions to Plasma Physics. 2007 Nov;47(7):551-8.
[39] Xie J, Chen Q, Suresh P, Roy S, White JF, Mazzeo AD. based plasma sanitizers. Proceedings of the National Academy of Sciences. 2017 May 16;114(20):5119-24.
[40] Misra NN, Moiseev T, Patil S, Pankaj SK, Bourke P, Mosnier JP, Keener KM, Cullen PJ. Cold plasma in modified atmospheres for post-harvest treatment of strawberries. Food and bioprocess technology. 2014 Oct 1;7(10):3045-54.
[41] Vaze ND, Gallagher MJ, Park S, Fridman G, Vasilets VN, Gutsol AF, Anandan S, Friedman G, Fridman AA. Inactivation of bacteria in flight by direct exposure to nonthermal plasma. IEEE Transactions on Plasma Science. 2010 Nov;38(11):3234-40.
[42] Eto H, Ono Y, Ogino A, Nagatsu M. Low-temperature sterilization of wrapped materials using flexible sheet-type dielectric barrier discharge. Applied physics letters. 2008 Dec 1;93(22):221502.
[43] Masaoka T, Kubota Y, Namiuchi S, Takubo T, Ueda T, Shibata H, Nakamura H, Yoshitake J, Yamayoshi T, Doi H, Kamiki T. Ozone decontamination of bioclean rooms. Appl. Environ. Microbiol.. 1982 Mar 1;43(3):509-13.
[44] Portugal, Sherlie E. "Design and improvement of dielectric barrier discharge (DBD) reactors for ozone generation in atmospheric air". PhD diss., University of Florida, 2018.
[45] Choudhury B, Portugal S, Mastanaiah N, Johnson JA, Roy S. Inactivation of Pseudomonas aeruginosa and Methicillin-resistant Staphylococcus aureus in an open water system with ozone generated by a compact, atmospheric DBD plasma reactor. Scientific Reports. 2018 Dec 4;8(1):17573.
[46] Portugal S, Roy S, Lin J. Functional relationship between material property, applied frequency and ozone generation for surface dielectric barrier discharges in atmospheric air. Scientific reports. 2017 Jul 25;7(1):6388.
[47] HYVAC PRODUCTS, INC., HYVAC. PressoVac-diaphragm pumps[online database] http://www.hyvac.com/PDFs/Literature/Pumps/PressoVac/Diagphram/PressoVac%20Diaphragm.PDF
[48] Vitality medicine. Medneb Compressor Nebulizer. [online database] https://www.vitalitymedical.com/medneb.html
[49] SKC.inc, Biostage Single-stage Impactor [online database] https://www.skcinc.com/catalog/index.php?cPath=400000000_401000000_401000100
[50] Sabersky RH, Sinema DA, Shair FH. Concentrations, decay rates, and removal of ozone and their relation to establishing clean indoor air. Environmental Science & Technology. 1973 Apr 1;7(4):347-53.
[51] 2B Technologies, Inc. Ozone Monitor Manual. 2B Technologies https://twobtech.com/docs/manuals/model_202_revJ.pdf. (2001).
[52] ANSYS FLUENT Theory Guide (2018)
[53] Singh KP, Roy S. Force approximation for a plasma actuator operating in atmospheric air. Journal of Applied Physics. 2008 Jan 1;103(1):013305
[54] Gupta AD, Roy S. Three-dimensional plasma actuation for faster transition to turbulence. Journal of Physics D: Applied Physics. 2017 Sep 22;50(42):425201

[55] Pasquarella C, Pitzurra O, Savino A. The index of microbial air contamination. Journal of hospital infection. 2000 Dec 1;46(4):241-56.
[56] Masati A, Sedwick RJ. Electrostatic forces acting on particle image velocimetry tracer particles in a plasma actuator flow. Journal of Applied Physics. 2018 Jan 7;123(1):014904.
[57] Hamdi M, Havet M, Rouaud O, Tarlet D. Comparison of different tracers for PIV measurements in EHD airflow. Experiments in fluids. 2014 Apr 1;55(4):1702.